The Conformation of Serum Albumin in Solution: A Combined Phosphorescence Depolarization-Hydrodynamic Modeling Study

M. Luisa Ferrer,* Ricardo Duchowicz,* Beatriz Carrasco,† José García de la Torre,† and A. Ulises Acuña*
*Instituto Química-Física "Rocasolano", Consejo Superior de Investigaciones Cientificas, 28006 Madrid, and †Departamento de Química-Física, Universidad de Murcia, 30071 Murcia, Spain

ABSTRACT There is a striking disparity between the heart-shaped structure of human serum albumin (HSA) observed in single crystals and the elongated ellipsoid model used for decades to interpret the protein solution hydrodynamics at neutral pH. These two contrasting views could be reconciled if the protein were flexible enough to change its conformation in solution from that found in the crystal. To investigate this possibility we recorded the rotational motions in real time of an erythrosin-bovine serum albumin complex (Er-BSA) over an extended time range, using phosphorescence depolarization techniques. These measurements are consistent with the absence of independent motions of large protein segments in solution, in the time range from nanoseconds to fractions of milliseconds, and give a single rotational correlation time ϕ(BSA, 1 cP, 20°C) = 40 $\pm$ 2 ns. In addition, we report a detailed analysis of the protein hydrodynamics based on two bead-modeling methods. In the first, BSA was modeled as a triangular prismatic shell with optimized dimensions of 84 $\times$ 84 $\times$ 84 $\times$ 31.5 Å, whereas in the second, the atomic-level structure of HSA obtained from crystallographic data was used to build a much more refined rough-shell model. In both cases, the predicted and experimental rotational diffusion rate and other hydrodynamic parameters were in good agreement. Therefore, the overall conformation in neutral solution of BSA, as of HSA, should be rigid, in the sense indicated above, and very similar to the heart-shaped structure observed in HSA crystals.

INTRODUCTION

Serum albumin is a highly soluble multidomain protein, without prosthetic groups or bulky appending carbohydrates, that is very stable and available at high purity and low cost (Peters, 1996). The fact that only relatively recently could a high-resolution x-ray image of the protein be obtained (He and Carter, 1992; Ho et al., 1993; Carter and Ho, 1994) made the human and bovine serum albumins (HSA and BSA) the subject of a wealth of physicochemical studies directed to the determination of the tertiary structure and solution conformation. Pioneering the field, Tanford, Scheraga, and their co-workers concluded that the protein in solution behaves as a compact spheroid particle (Tanford and Buzzel, 1956; Loeb and Scheraga, 1956), as was also iterated in additional hydrodynamic studies (e.g., Champagne, 1957). However, this representation was later replaced by the standard, textbook hydrodynamic model of BSA: a cigar-shaped ellipsoid with dimensions of 140 $\times$ 40 Å and axial ratio of $\sim$3.5, with three domains in line (Fig. 1 *a*). That model was claimed (Squire et al., 1968; Peters, 1996) to be consistent with a series of measurements of sedimentation, dielectric dispersion, electric birefringence, low-angle x-ray scattering, and transmission electron microscopy. It also received some support from the images recorded by scanning tunneling microcopy (Feng et al., 1989) and is still frequently used (Peters, 1996; Durchslang and Zipper, 1997, Matulis et al., 1999). Even more, the first low-resolution crystallographic data of HSA were initially analyzed as such a linear structure (Carter et al., 1989), soon to be abandoned in favor of the current heart-shaped conformation (Carter and He, 1990; He and Carter, 1992; Carter and Ho, 1994) (Fig. 1 *b*). Interestingly, Carter and Ho (1994) noted that conflicting reports questioning the cigar-shaped paradigm were dismissed without much consideration. That was the case, e.g., of the dark-field electron micrographs of the homologous human and bovine α-fetoprotein (Luft and Lorscheider, 1983) or the results of resonance energy transfer experiments (Hagag et al., 1983), which could only be explained by a structure similar to that Fig. 1 *b*.

The two disparate views of serum albumin conformation might be reconciled if the tertiary structure of the protein in the crystal is different from that in solution. It was initially speculated that the presence of residual associated fatty acids in the solution preparations, which are absent in the de-lipidated crystals, would favor that change. However, recent x-ray structures of HSA, both without (Sugio et al., 1999) and with (Curry et al., 1998) associated myristic acid, show that although important domain rotations are observed in the last case, the overall protein profile is essentially preserved. Alternatively, one may think of a soft flexible protein structure that adopts a folded conformation within the crystalline environment. Prompted by this discrepancy we wished to revise the hydrodynamic information that is obtained from the depolarization of the protein luminescence (fluorescence and phosphorescence). With these optical techniques the rotational motions of a macromolecule in solution can be monitored in real time (Lakowicz, 1999), and important information on the flexibility of its structure can also be obtained (Munro et al., 1979). In this way it has

Received for publication 17 July 2000 and in final form 30 January 2001.
Address reprint requests to Dr. A.Ulises Acuña, Instituto Química-Física "Rocasolano", CSIC, 119 Serrano, 28006 Madrid, Spain. Tel.: 34-91-561-9400; Fax: 34-91-564-2431; E-mail: roculises@iqfr.csic.es.
© 2001 by the Biophysical Society
0006-3495/01/05/2422/09 $2.00

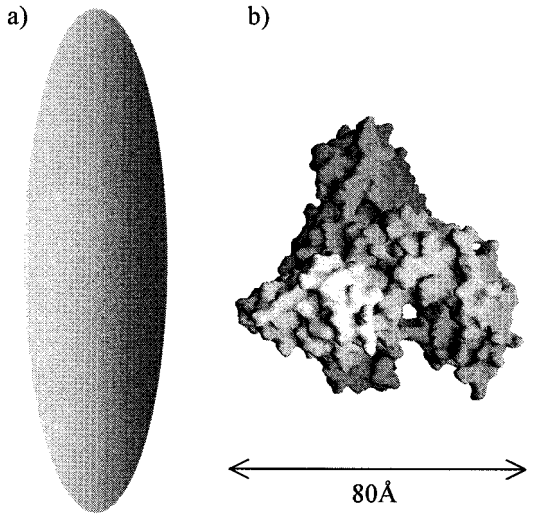

FIGURE 1 (*a*) The elongated ellipsoid (140 × 40 Å) used frequently to model the conformation in solution of human and bovine serum albumin; (*b*) An image of HSA at the same scale, adapted from the Brookhaven Protein Data Bank x-ray coordinates file1bm0 (Sugio et al., 1999).

been observed that the time-resolved depolarization of the intrinsic fluorescence (tryptophan) of serum albumin (Munro et al., 1979; Gentiu et al., 1990; Marzola and Gratton, 1991; Lakowicz and Gryzynski, 1992; Helms et al., 1997) contains a very fast decay time (140–500 ps), due to the localized motion of the emitting residue, and a much slower one (34–40 ns) corresponding to the global Brownian rotation of the protein. Although the last value is difficult to determine with accuracy due to the short fluorescence lifetime of tryptophan, these experiments give a hint as to the absence of internal motions of large protein domains, at least in the tens of nanoseconds range. Furthermore, Castellano et al. (1998) succeeded in linking a long lifetime (~800 ns) Ru(II) label to HSA and measured a very accurate single rotational correlation time of 41 ns. The accessible time window can be extended further still by the phosphorescence depolarization methods introduced by Garland and Moore (1979). In this way, values of the rotational time of HSA in viscous solvents were determined (Hustedt et al., 1993; Marriott et al., 1994) that, if extrapolated back to 1 cP and 20°C, are coincident with those recorded above. It is important to remark that these studies, which were not concerned with the solution conformation of the protein, provide an unbiased record of its diffusive motions obtained with three different luminescent labels.

For the present work we selected the phosphorescence depolarization of erythrosin bound to BSA to reanalyze the hydrodynamics of the protein, because of its potential to explore the reorientational Brownian motions over an unprecedentedly broad time-range, from hundreds of nanoseconds to milliseconds. In addition, we profited from a recent characterization (Duchowicz et al., 1998) of several spectroscopic parameters of the dye relevant to this study. These experiments, combined with the computation of the solution hydrodynamic properties of the protein carried out by recently developed bead-modeling methods, show that the heart-shaped x-ray structure of albumin (Fig. 1 *b*) is also the most likely conformation in solution of BSA at neutral pH, with no indication of independent motions of large domains in the nanosecond to millisecond time range.

MATERIALS AND METHODS

Materials

Erythrosin (2′,4′,5′,7′-tetraiodofluorescein) sodium salt (>99%; Scharlau, Barcelona, Spain) was recrystallized several times from methanol/hexane mixtures and its purity checked by thin-layer chromatography. Glycerol and sodium mono- and dihydrogen phosphate (>99%; Merck, Darmstadt, Germany) were used as received. Samples of lyophilized BSA (>99%; Fluka, Ronkonkoma, NY) were dissolved in 10 mM phosphate buffer (pH 7.4) and found free of impurities and aggregates by electrophoresis, analytical ultracentrifugation, and absorption spectroscopy. Before spectroscopic measurements, the solutions were degassed by bubbling purified Argon (<5 ppm O_2), which had been passed through an Oxy-Trap column (Alltech, Deerfield, IL) to further reduce the oxygen content.

Glycerol/water mixtures

The composition (w/w) and viscosity (Poise) of the glycerol/buffer mixtures was determined from the measured refractive index (20°C) and tabulated values (Miner and Dalton, 1953; Litovitz, 1952; West, 1982). The viscosity for temperature values not included in these tabulations was found by interpolation from a plot of Andrade's equation (Litovitz, 1952) $\eta = \eta_0 \exp \Delta E/kT$, where ΔE is the activation energy of the viscous flow. For the glycerol/water compositions (82–92%) and temperatures (273–300 K) used here we found $\Delta E = 13$ kcal mol^{-1}.

Erythrosin binding to BSA

A 10^{-6} M solution of erythrosin in phosphate buffer (pH 7.4) was mixed with BSA to form the noncovalent complex, as in Garland and Moore (1979). The absorption maximum of the protein-bound dye shifted 13 nm to the red, from $\lambda_{free} = 527$ nm to $\lambda_{bound} = 540$ nm, but there were only minor changes in band shape and absorption coefficient (~8.5×10^4 M^{-1} cm^{-1}). The binding process was monitored as a function of the relative concentration of dye and protein, from the fractional shift of the absorption maximum on erythrosin $\Gamma = (\lambda - \lambda_f)/(\lambda_f - \lambda_b)$, where λ is the peak absorption of the protein/dye mixture. The inset of Fig. 2 shows a typical experiment, where it can be observed that for 1:1 erythrosin-protein ratio all the dye is in the bound form. The solutions used in the glycerol/buffer mixtures contained a 10-fold excess of BSA to keep the free dye concentration negligible.

Spectroscopic methods

Absorption measurements were recorded by a Varian-Cary 290 spectrophotometer. Stationary fluorescence and phosphorescence spectra were obtained with a modified SLM 8000D fluorimeter and corrected for the wavelength sensitivity of the detection system. Time-resolved measurements of phosphorescence were carried out with a laser spectrometer fully described elsewhere (Duchowicz et al., 1998). In short, pulses (532 nm, <0.5 mJ, 15 ns, 20 Hz) from a Molectron MY-34 Nd:YAG Q-switched laser were used to excite the emission from degassed, thermostatted samples. The linear polarization of the laser pulse was selected with a Glan-

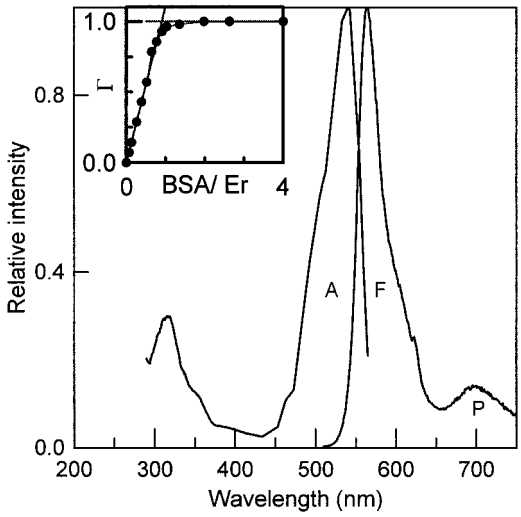

FIGURE 2 The absorption (A), fluorescence (F), and phosphorescence (P) spectra of the 1:1 noncovalent erythrosin-BSA complex in glycerol/phosphate buffer (10^{-6} M, 82.5% w/w, pH 7.4, 20°C, λ_{exc} = 480 nm). (*Inset*) Plot of the relative wavelength shift of the absorption maximum of the dye Γ versus BSA/erythrosin ratio, for a 10^{-6} M dye solution in phosphate buffer, pH 7.4 (see Materials and Methods).

Taylor polarizer and a Fresnel rhomb rotator. Phosphorescence emitted at 90° to the excitation beam was focused on a Thorn-EMI 9816 photomultiplier through an additional polarizer and a set of filters, the latter to attenuate scattered laser light and dye fluorescence. A specially built photomultiplier gating circuit (Yoshida et al., 1989; Herman et al. 1992) prevented the distortion of kinetic signals at early times. Decay traces were digitized (2000 channels), displayed, and averaged ($>10^3$ times) with a Phillips 3320 oscilloscope. The overall instrumental resolution was ~100 ns, with a gating dead time of 300 ns. Time-resolved phosphorescence depolarization experiments are very sensitive to saturation effects that yield anomalous low values of the initial anisotropy (see Peng and Barisas, 1997, for a detailed account). Here we used a solid polymethyl methacrylate (PMM) solution of erythrosin to select the appropriate linear range of laser excitation energies (r_0[Er-PMM] = 0.25).

Analysis of phosphorescence lifetime and depolarization

The decay of the total phosphorescence intensity, recorded with the emission polarizer set at the magic angle $m = 54.7°$ relative to the vertically polarized laser beam, was fitted (without deconvolution) to a sum of exponentials by standard nonlinear least-squares methods developed locally (Mateo et al., 1991): $I_m(t) = \Sigma a_i \exp(-t/\tau_i)$. It was found experimentally that the noise can be approximated to within a scale factor by a Poisson distribution, i.e., $\sigma_i = [I(t)]^{1/2}$.

The anisotropy $r(t)$ of the phosphorescence was computed by recording the emission intensities parallel $I_\parallel(t)$ and perpendicular $I_\perp(t)$ to the vertically polarized exciting pulses:

$$r(t) = \frac{I_\parallel(t) - GI_\perp(t)}{I_\parallel(t) + 2GI_\perp(t)} \tag{1}$$

where G is a factor determined experimentally that compensates for the polarization bias of the detection setup. The absence of systematic errors was checked by comparing the fitted functions of $I_m(t)$ with that of the sum $I_\parallel(t) + 2GI_\perp(t)$, proportional to the total emission intensity. The decay of $r(t)$ was analyzed with the expression describing the rotational emission depolarization of a rigid symmetric top (prolate-oblate ellipsoids of revolution) (Chuang and Eisenthal, 1972; Ehrenberg and Rigler, 1972; Belford et al., 1972):

$$\begin{aligned} R(t) = r(t)/r_0 = {} & \alpha_1 \exp - t/\phi_1 \\ & + \alpha_2 \exp - t/\phi_2 + \alpha_3 \exp - t/\phi_3 \end{aligned} \tag{2}$$

where r_0 is the intrinsic anisotropy and the pre-exponentials α_i depend only on the relative orientation of the electronic transition moments of the emitting label. This expression can be used also, more generally, for any object with an axis of ternary or higher symmetry, as the BSA models used here. In the case of a protein randomly labeled with an emitting dye $\alpha_1 = \alpha_2 = 2\alpha_3 = 2/5$. The rotational correlation times ϕ_i (s^{-1}) are related to the rotational diffusion coefficients of the ellipsoid $D_\parallel$ and $D_\perp$ by $\phi_1 = (4D_\parallel + 2D_\perp)^{-1}$, $\phi_2 = (D_\parallel + 5D_\perp)^{-1}$, and $\phi_3 = (6D_\perp)^{-1}$. Moreover, it is known that in this case the $r(t)$ decay recorded experimentally would be very close to a single exponential function for prolate ellipsoids with axial ratio $p \leq 5$ and for any oblate ellipsoid (Small and Isenberg, 1977; Wahl, 1983). Recognizing this limitation, we fit the observed decay to an approximate function with an average correlation time ϕ_{av}:

$$r(t)_{av} = r_0 \exp(-t/\phi_{av}), \tag{3}$$

which shares with the exact function (Eq. 2) the following properties: 1) the value at $t = 0$ and at $t = \infty$ are the same, and 2) the area enclosed by the two functions is also the same. According to that we obtain

$$\int_0^\infty r(t)dt = \int_0^\infty r(t)_{av}dt \tag{4}$$

and

$$\phi_{av} = \sum_1^3 \alpha_i \phi_i. \tag{5}$$

Numerical simulations incorporating realistic noise levels (not shown) indicate that, in fact, this approximate function cannot be distinguished from the exact one for prolate and oblate ellipsoids randomly labeled with axial ratios $p < 4$ and $p > 0.2$, respectively. Note that the ϕ_{av} as defined in Eq.5 is different from the harmonic mean value that obtains from the slope of the $r(t)$ function at $t = 0$ (Wahl, 1983). The anisotropy fitting routines were also based on the nonlinear least-squares methods, as above.

The dependence of the diffusion coefficients on molecular size, geometry, short-range solvent interactions, and temperature can be expressed for a symmetric top in a compact way by the Stokes-Einstein-Debye equation, which for stick boundary conditions takes the form (Mateo et al., 1993):

$$D_i = kT/6\eta V g_i \quad (i \rightarrow \parallel, \perp) \tag{6}$$

where V is the hydrodynamic volume and η the solvent viscosity. The Perrin factors g_i (Perrin, 1934) depend only on the axial ratio of the ellipsoid $p = a/b$ (where a is the symmetry axis) and are given by

$$\begin{aligned} g_\parallel &= 2(p^2 - 1)/[3p(p - S)] \\ g_\perp &= 2(p^4 - 1)/[3p(2p^2 - 1)S - p] \end{aligned} \tag{7}$$

$$\begin{aligned} S_{PROL} &= (p^2 - 1)^{-1/2} \ln[p + (p^2 - 1)^{1/2}] \\ S_{OBL} &= (1 - p^2)^{-1/2} \text{arctg}[p^{-1}(1 - p^2)^{-1/2}] \end{aligned} \tag{8}$$

RESULTS

Phosphorescence lifetime of Er-BSA

The decay of the phosphorescence of the Er-BSA complex in the glycerol/buffer mixtures used here (82–92% w/w), in the temperature range 273–291 K, is mono-exponential over a range of 2 ms (Fig. 3) with a lifetime of 420 ± 20 μs (273 K). A small fraction of a faster component (~20 μs) can be detected only when the first 100 μs of the decay are recorded at the highest time-resolution available, 125 ns/channel (Table 1). Because the phosphorescence lifetime of the free dye is strictly mono-exponential and very sensitive to solvent polarity (Duchowicz et al., 1998), this second component may be due to a small fraction of the BSA-dye complexes in which the dye is located in a different microenvironment. According to that, the Er-BSA samples appear structurally very homogeneous. This is an important requirement for the following analysis of the decay of the anisotropy.

Rotational depolarization of the Er-BSA phosphorescence

The decay of the phosphorescence anisotropy of Er-BSA was measured as a function of viscosity (4–19 Poise) by changing the glycerol concentration in isothermal conditions. In addition, a set of measurements was carried out as a function of temperature for the 92% w/w solution. If independent reorientational modes are present, increasing the temperature results in a decay of the optical anisotropy faster than expected from the lowering of the viscosity, and frequently new exponential terms become evident, due to the enhanced amplitude of the segmental motions. However, in all the cases, $r(t)$ could be fitted to a single-exponential function, with a random and even distribution of weighted residuals with, therefore, no indication of motions from individual domains (Table 2). A representative trace (Fig. 4) shows that the decay could be followed with a good S/N ratio for a range of more than three time constants. On the other hand, the value at $t = 0$ of the anisotropy, $r(0) \approx 0.1$, differs substantially from the r_0 value of free erythrosin immobilized in PMM (0.25), which was determined here with the same spectrometer (Duchowicz et al., 1998) and by others in different conditions (Garland and Moore, 1979; Lettinga et al., 1999). Therefore, the decrease in the initial anisotropy should be due to unresolved sub-microsecond motions of the dye within its protein-binding pocket.

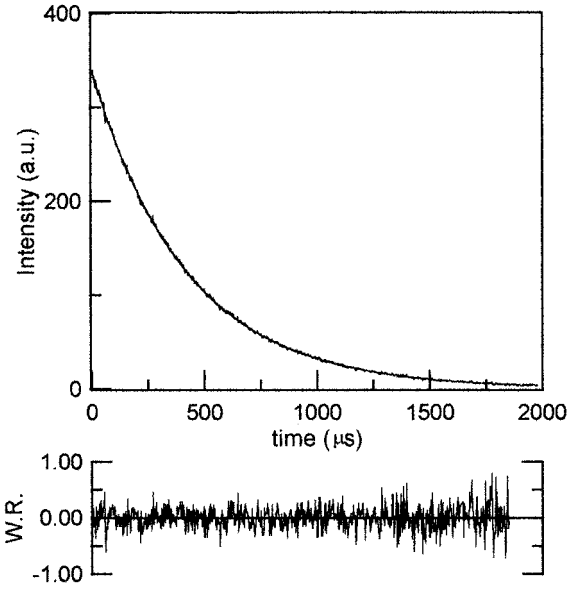

FIGURE 3 The decay of the phosphorescence intensity of the erythrosin-BSA complex and the fitted monoexponential function, with a phosphorescence lifetime $\tau_p = 421 \pm 20$ μs (10^{-7} M, 92% w/w glycerol/buffer, 0°C, 2.5 μs/channel).

TABLE 1 Phosphorescence lifetime of the erythrosin-BSA complex, 10^{-7} M, in glycerol/buffer mixtures at constant temperature $T = 273$ K

% Glycerol	η/P	$a_1 \pm 0.02$	τ_1/μs	$a_2 \pm 0.02$	τ_2/μs	χ^2
92.0	18.6	0.06	16 ± 2	0.94	421 ± 20	0.02
90.5	13.4	0.06	20 ± 2	0.94	400 ± 40	0.02
86.5	7.0	0.06	22 ± 2	0.94	445 ± 40	0.02
83.0	4.0	0.07	7 ± 2	0.93	417 ± 42	0.02

Time range, 100 μs; 0.125 μs/channel.

DISCUSSION

The rotational correlation time of BSA

The kinetics of the optical anisotropy decay of Er-BSA depends on the protein size and shape as well as on the orientation of the dye electronic transition moments relative to the protein inertial axis. In this case it is observed that the dye reorients much faster than the protein to attain in nanoseconds an equilibrium angular distribution characterized by the value $r(0) \approx 0.1$. This initial anisotropy is finally averaged out to zero by the global tumbling (ϕ) of the protein. The amplitude of the independent motions of the

TABLE 2 Phosphorescence anisotropy decay parameters of the erythrosin-BSA complex, 10^{-6} M, in glycerol/buffer mixtures

% Glycerol	T/K	η/P	$r(0) \pm 0.01$	ϕ/μs	χ^2
92.0	291	4.0	0.07	16 ± 1.5	0.003
92.0	284	5.8	0.09	21 ± 1.5	0.002
92.0	283	8.0	0.09	35 ± 2.5	0.003
92.0	279	12.0	0.10	47 ± 3.0	0.002
92.0	273	18.6	0.07	67 ± 5.0	0.003
90.5	273	13.4	0.08	58 ± 4.0	0.020
86.5	273	7.0	0.08	34 ± 2.0	0.020
83.0	273	4.0	0.10	19 ± 1.5	0.020

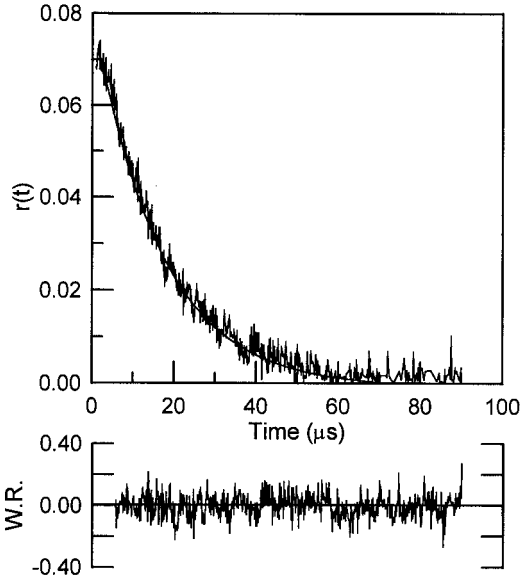

FIGURE 4 The decay of the phosphorescence anisotropy of the erythrosin-BSA complex and the fitted monoexponential function, with a rotational correlation time $\phi = 16 \pm 1.5$ μs (10^{-6} M, 92% w/w glycerol/buffer, 18°C, 0.25 μs/channel).

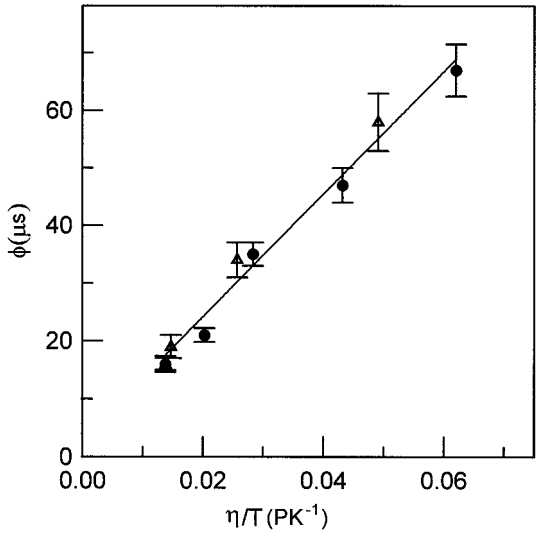

FIGURE 5 Rotational correlation time of the erythrosin-BSA complex in different mixtures of glycerol/buffer as a function of η/T, measured by phosphorescence depolarization at 273 K constant temperature (●) or at 92% w/w glycerol constant composition (▲). The value of ϕ extrapolated to 1 cP, 273 K is 40 ± 2 ns.

dye can be estimated assuming (Kinosita et al., 1977) that the emitting dipole moves freely within a cone of semi-angle θ_0. In that case the observed ratio $r(0)/r_0 = 0.4$ corresponds to $\theta_0 \approx 50°$. Because the phosphorescence emission dipole is placed 40° relative to the long erythrosin axis (Lettinga et al., 1999), the three-ring xantene system oscillates with large-amplitude motions, producing a nanoseconds dynamic averaging of its orientation relative to the protein. For the present purposes, it is enough to consider the protein molecules as a population over which the mean dye orientations are distributed randomly. This assumption is not essential for the following discussion but simplifies considerably the algebraic manipulation. Thus, the rotational motions of BSA approximated by those of an ellipsoid have an average correlation time (see Materials and Methods) given by

$$\phi_{av} = 0.4\phi_1 + 0.4\phi_2 + 0.2\phi_3. \tag{9}$$

By replacing in Eq. 9 the values of the diffusion coefficients D_i we get

$$\begin{aligned} \phi_{av} &= \frac{6\eta V}{kT}\,\Pi \\ \Pi &\equiv \left[\frac{0.4}{2g_\perp^{-1} + 4g_\parallel^{-1}} + \frac{0.4}{5g_\perp^{-1} + g_\parallel^{-1}} + \frac{0.2}{6g_\perp^{-1}}\right] \end{aligned} \tag{10}$$

The plot of ϕ_{av} values of Er-BSA as a function of η/T is presented in Fig. 5. The linearity of this plot confirms the validity of the Stokes-Einstein-Debye approximation in these experiments and indicates that the size (V) and conformation (g_i) of the protein (whatever they are) remain constant for all the temperature-viscosity conditions. The BSA correlation time in buffer solution extrapolated from these data would be ϕ (1 cP, 20°C) = 40 ± 2 ns. Finally, by replacing η in Eq. 10 by the expression given in Andrade's equation we get

$$\phi_{av} = \frac{6\eta_0 V}{kT}\,\Pi \exp(\Delta E/kT). \tag{11}$$

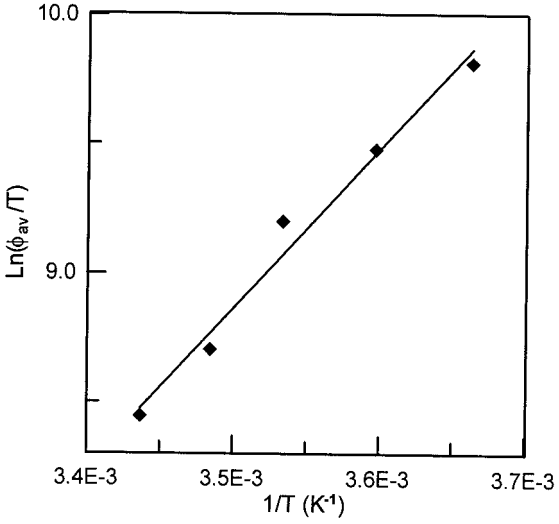

FIGURE 6 Plot of $\ln(\phi_{av}T)$ versus $1/T$ (Eq. 11 in the text) for the erythrosin-BSA complex in glycerol/buffer (10^{-6} M, 92% w/w).

The plot of ln ($\phi_{av}T$) versus $1/T$ is linear (Fig. 6) with a slope $\Delta E = 13$ kcal mol^{-1}. The coincidence of this value with the activation energy of the viscous drag of glycerol (see above) is also an indication that the observed correlation time corresponds to Brownian motions of the whole protein, damped by the macroscopic viscosity of the solvent. In summary, from these results together with the previous measurements of optical anisotropy carried out with a diversity of luminescent probes reviewed above (Introduction), it can be concluded that the overall solution conformation of human and bovine serum albumin is very similar, with no indication of domain flexibility over a large time range, from nanoseconds to fractions of milliseconds.

The shape of BSA in solution

The classical approach based on rigid symmetric tops

The simultaneous analysis of several hydrodynamic properties in terms of solids of revolution, such as spheres and ellipsoids, is a way to get an idealized shape and size of proteins in solution (for reviews see Cantor and Schimmel, 1980; Harding, 1995). In the case of BSA, the outcome of many of these analyses resulted in the elongated shape of Fig. 1 *a*. However, it is shown below from very simple considerations that this model is very unlikely. For that purpose we use the rotational correlation time ϕ established above and the intrinsic viscosity [η] of BSA, because the majority of the BSA [η] values found in the literature fall within the interval 3.92–4.21 cm^3 g^{-1}, as determined by McMillan (1974) in a critical assessment of five experimental methods. We take [η] BSA (pH 7, 20°C) = 4.1 ± 0.1 cm^3 g^{-1}. For ellipsoids of revolution, the intrinsic viscosity can be expressed (Harding, 1995) as $[\eta] = \nu N_A V/M$, where M is the molecular mass of the protein, N_A the Avogadro constant, and ν the so-called Simha factor that depends only on the ellipsoid axial ratio (Montejo et al., 1992). The expression for the average correlation time can now be written in a convenient form as

$$\phi_{av} = \frac{6\eta[\eta]M}{RT}\,\nu^{-1}\Pi, \qquad (12)$$

where the product $\nu^{-1}\Pi$ depends only on the axial ratio of the idealized particle. Therefore, given a set of experimental values of the intrinsic viscosity of the protein, its molecular mass, and the solvent viscosity one can use Eq. 12 to compute the expected rotational correlation time ϕ_{av} for a series of values of the axial ratio. Note that Eq. 12 applies to the case of the random distribution of the emitting dye. Fig. 7 shows a plot of the expected correlation times for BSA (1 cP, 20°C), using the above range of values of the intrinsic viscosity, the known molecular mass (66,500 g mol^{-1}; Peters, 1996), and tabulated values of Perrin and Simha factors (Harding, 1995). It can be concluded that the standard elongated shape of Fig. 1 *a* ($p = 3.5$) is not the best choice to account for the experimental values of ϕ and [η]. Moreover, the BSA conformation appears difficult to idealize by any biaxial ellipsoid, so the spheroid shape initially proposed by Tanford, Scheraga, and their co-workers was the more appropriate simplification. Nowadays, one can use models with atomic detail to obtain accurate hydrodynamic information, as shown below.

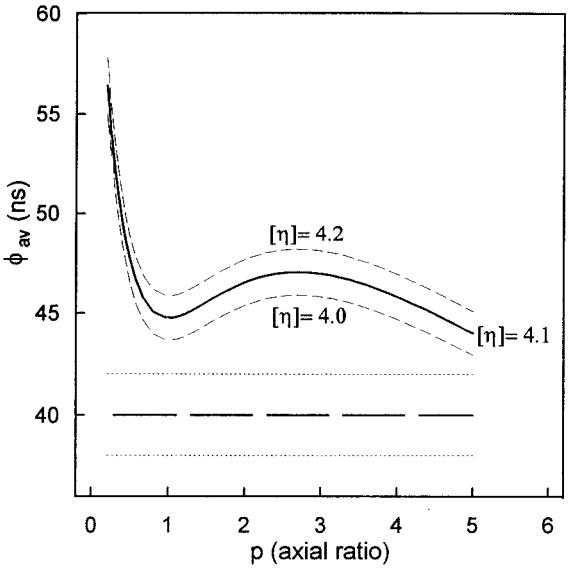

FIGURE 7 The expected average correlation time ϕ_{av} (1 cP, 20°C) of ellipsoidal models of BSA as a function of the axial ratio p (oblate $p < 1$ and prolate $p > 1$). The values of ϕ_{av} were computed from Eq. 12, keeping constant the protein intrinsic viscosity [η] = 4.1 ± 0.1 cm^3 g^{-1}, as described in the text. The rotational correlation time expected for the elongated model ($p = 3.5$) of Fig. 1 *a* is ~46 ns, which differs significantly from the experimental value (40 ± 2 ns), indicated here by the horizontal lines.

Bead modeling of BSA hydrodynamics with a triangular shell

The rotational diffusion coefficients, as well as any other hydrodynamic property of a solid particle with an arbitrary shape, can be computed by the methods of bead modeling initially proposed by Bloomfield et al. (1967) and further developed by García de la Torre and co-workers (García de la Torre and Boomfield, 1981; García de la Torre et al., 1994; Carrasco and García de la Torre, 1999). These methods are applied here to compute a set of solution properties of BSA and provide an example of the newest bead-modeling strategies (Carrasco and García de la Torre, 1999).

The particle representing the protein conformation in solution is taken as a solid equilateral triangular prism (Fig. 8 *a*), with dimensions 80 × 80 × 80 × 30 Å, as suggested for crystalline HSA (He and Carter, 1992). In a first step, the prism volume is filled with small beads of radius σ, typi-

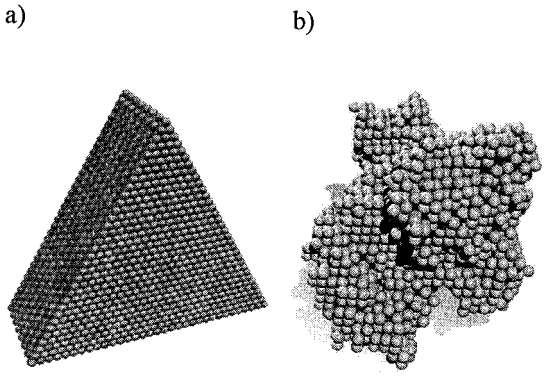

FIGURE 8 (*a*) Rough shell triangular model of BSA with dimensions of 80 × 80 × 80 × 30 Å; (*b*) Rough shell model derived from the atomic-level structure of HSA (PDB file 1bm0; Sugio et al., 1999)

cally 1–3 Å. To do so, the prism is immersed in a closest-packed hexagonal lattice and beads of 2σ diameter, equal to the lattice spacing, are placed at the lattice nodes falling within the particle. In the next step, all the internal beads are removed (those fully surrounded by 12 beads, the lattice coordination number). In this way, one obtains the so-called rough shell model (Fig. 8 *a*), which is next used as the input for the HYDRO computer program (García de la Torre et al. 1994). These computations are carried out for several values of σ and the parameters extrapolated to the shell-model limit $\sigma \rightarrow 0$. To take into account the particle expansion due to hydration we carried out calculations for several particle sizes given by $80f \times 80f \times 80f \times 30f$, where f is a factor close to unity. Note that in this way the shape of the hydrated particle is preserved and only the absolute dimensions are varied.

The results for the shell model are listed in Table 3 as the translational diffusion coefficient D_t, rotational correlation time ϕ_i, intrinsic viscosity $[\eta]$, and sedimentation coefficient s. Note that the five rotational correlation times expected for an arbitrary shape reduce to three for this particular case, due to the threefold axial symmetry of the particle. These values were used to compute ϕ_{av} with Eq. 9. The experimental rotational correlation time obtained in this work, as well as the rest of the BSA hydrodynamic parameters, are reproduced to a good approximation for $f = 1.05$, corresponding to rigid particle dimensions of 84 × 84 × 84 × 31.5 Å. According to this, the conformation of BSA in neutral solution is fairly consistent with that of HSA in the crystal.

Bead modeling of BSA hydrodynamics with atomic-level HYDROPRO computations

The hydrodynamic properties of proteins can be accurately predicted from atomic-level structures derived from the atomic coordinates of a Protein Data Bank (PDB)-formatted file, as has been shown recently (García de la Torre et al., 2000). Using as input the PDB file and some elementary properties of the macromolecule and the solvent, the computer program HYDROPRO provides a full set of solution properties. The availability of atomic coordinates of HSA (PDB file 1bm0; Sugio et al., 1999) makes possible an analysis of the properties of serum albumin using this method, of which a new example of applicability is thus provided.

In atomic-level hydrodynamic modeling, each non-hydrogen atom is represented by a spherical element. The atomic-element radius, a, identical for all the atoms, has a minimum value corresponding to the mean van der Waals radius of the protein atoms, ~1.8 Å. Slightly larger values of a may be found due to protein hydration. In practice, a is regarded as an adjustable parameter, although it is allowed to vary only within a narrow, physically significant range. In practical calculations, a series of values of a is considered, for instance 2, 3, and 4 Å. The array of atomic spherical elements, with some fixed value of a, is the primary hydrodynamic model (García de la Torre et al., 2000). In the primary hydrodynamic model there is consid-

TABLE 3 Hydrodynamic parameters calculated for the rough shell model of the equilateral triangular representation (Fig. 8 *a*) of BSA

Model parameter			Calculated property						
Side/Å	Thickness/Å	f	$D_t \times 10^7$/cm^2 s^{-1}	$[\eta]$/cm^3 g^{-1}	s/S	ϕ_1/ns	ϕ_2/ns	ϕ_3/ns	ϕ_{av}/ns
80.0	30.0	1.00	6.63	3.04	4.85	35.6	36.3	44.0	38
82.0	30.8	1.025	6.47	3.27	4.70	38.3	39.1	47.3	40
84.0	31.5	1.05	6.31	3.52	4.59	41.2	42.0	50.9	43
86.0	32.3	1.075	6.17	3.78	4.48	44.2	45.1	54.6	47
88.0	33.0	1.10	6.03	4.05	4.38	47.3	48.3	58.5	50
90.0	33.8	1.125	5.89	4.33	4.28	50.6	51.7	62.6	53
92.0	34.5	1.15	5.77	4.62	4.19	54.1	55.2	66.9	57
			6.27*	**4.1 ± 0.1**†	**4.60***				**40 ± 2**‡

Numbers in bold are experimental values (water, 20°C).
*Philo, 1994.
†McMillan, 1974.
‡This work.

TABLE 4 Hydrodynamic parameters of BSA calculated by HYDROPRO from the PDB file 1bm0 (HSA monomer), for different values of the radius *a* of the atomic elements in the primary hydrodynamic model (Fig. 8 *b*)

Atomic radius	Calculated property								
a (Å)	$D_t \times 10^7/\mathrm{cm}^2\ \mathrm{s}^{-1}$	$[\eta]/\mathrm{cm}^3\ \mathrm{g}^{-1}$	s/S	θ_1/ns	θ_2/ns	θ_3/ns	θ_4/ns	θ_5/ns	ϕ_{av}/ns
2.0	6.28	3.63	4.64	37.8	38.3	40.9	44.6	45.1	40
3.0	6.03	4.09	4.45	42.6	43.1	46.4	50.0	50.7	45
4.0	5.78	4.63	4.27	48.4	48.9	52.4	56.5	57.2	51

erable overlap of the spheres, and therefore, it is not suitable for direct bead-model calculations. Instead, the set of overlapping spheres is taken as the solid particle to which the general procedure of shell modeling can be applied, as for the triangular prism in the preceding section. As there, the primary hydrodynamic model is filled with closest-packed minibeads of radius σ, and those fully surrounded by the maximum (coordination) number of beads are removed, to give the final shell model, shown in Fig. 8 *b*. This is the model used as input for HYDRO for the computation of the solution properties, again as extrapolated to the shell-model limit of $\sigma = 0$. The results from this computation based on the crystallographic structure of HSA taken from the PDB file 1bm0 (monomer) are given in Table 4.

The values of the properties for intermediate values of a, or values of a corresponding to a given value of some property, can be easily determined by interpolation in Table 4. The five correlation times (θ_1–θ_5) are very similar and, in addition, show the expected relationship $\theta_1 \approx \theta_2$ and $\theta_4 \approx \theta_5$. Thus, to get a ϕ_{av} value to be compared with the experimental one (40 ± 2 ns) we used Eq. 9 and the mean values $\phi_1 = (\theta_1 + \theta_2)/2$, $\phi_2 = (\theta_4 + \theta_5)/2$ and $\phi_3 = \theta_3$, according to the axis definition of the rotating particle. The agreement with the experimental values for $a = 2$ Å is very satisfactory, particularly when we consider that the calculation has been carried out using directly the atomic structure with standard values of the a parameter. An even better agreement might be obtained on adjustment of the value of a to fit best the set of experimental parameters. These model predictions again give strong support to the similarity between the BSA conformation in solution and the HSA crystal structure.

In acid solution, the compact HSA structure probably unfolds to a more extended one, as proposed by Carter and Ho (1994). Because the corresponding acid form of BSA is indeed well represented by an elongated ellipsoid (Bloomfield, 1966) one might speculate that this property may well have contributed to the long-standing preference for elongated hydrodynamic models for the protein.

CONCLUSIONS

The decay of the optical anisotropy of the erythrosin-BSA complex recorded over a large time range by phosphorescence techniques in glycerol/buffer mixtures, both in isothermal and non-isothermal conditions, is monoexponential and correlates quantitatively with that found in aqueous buffers. At neutral pH, therefore, the protein maintains a well-defined overall conformation without signs of large-domain flexibility over a time range from nanoseconds to fractions of milliseconds.

The simultaneous analysis, in terms of solid symmetric tops, of the intrinsic viscosity of BSA and its rotational correlation time obtained here, show that the choice of the standard elongated shape to idealize the protein in solution is inappropriate.

On the other hand, the detailed computation of the hydrodynamic properties of the protein with recently developed bead-model methods supports a stiff compact conformation in neutral solution for BSA, as well as of HSA, very similar to the heart-shaped structure of the latter observed in the crystal.

The phosphorescence fitting routines were based on programs developed by Dr. M. P. Lillo, whose contribution and criticisms are gratefully acknowledged. We are also indebted to Dr. R. E. Dale for essential advice, to Dr. F. Amat-Guerri for erythrosin purification, to Dr. M. Martínez-Ripoll for his help in image design, and to Drs. A.P. Minton and G. Rivas for helpful comments. S. Leineweber, at the Max-Planck Institute of Biophysical Chemistry, Göttingen, Germany, built the PM gating circuit under the invaluable guidance of Prof. T. M. Jovin. R.D. acknowledges the support of a sabbatical grant, and M.L.F. of a fellowship from the Spanish Dirección General de Investigación Científica y Técnica (DGICYT). B.C. acknowledges a post-doctoral fellowship from Caja Murcia.

This work was financed by projects PB96–852 and PB96–1106 from the DGICYT and grant 01578/CV/98 from the Fundación Séneca (Región de Murcia).

REFERENCES

Belford, G. G., R. L. Belford, and G. Weber. 1972. Dynamics of fluorescence polarization in macromolecules. *Proc. Natl. Acad. Sci. U.S.A.* 69:1392–1393.

Bloomfield, V. A. 1966. The structure of bovine serum albumin at low pH. *Biochemistry.* 5:684–689.

Bloomfield, V. A., W. O. Dalton, and K. E. Van Holde. 1967. Frictional coefficients of multisubunit structures. I. Theory. *Biopolymers.* 5:135–148.

Cantor, C. R., and P. R. Schimmel. 1980. Biophysical Chemistry. V. H. Freeman and Co, San Francisco.

Carrasco, B., and J. García de la Torre. 1999. Hydrodynamic properties of rigid particles: comparison of different modeling and computational procedures. *Biophys. J.* 75:3044–3057.

Carter, D. C., and X. M. He. 1990. Structure of human serum albumin. *Science.* 249:302–304.

Carter, D. C., X. M. He, S. H. Munson, P. D. Twigg, K. M. Gernet, M. B. Broom, and T. Y. Miller. 1989. Three-dimensional structure of human serum albumin. *Science.* 244:1195–1198.

Carter, D. C., and J. X. Ho. 1994. Structure of serum albumin. *Adv. Protein Chem.* 45:153–196.

Castellano, F. N., J. D. Dattelbaum, and J. R. Lakowicz. 1998. Long-lifetime Ru(II) complexes as labeling reagents for sulfhydryl groups. *Anal. Biochem.* 255:165–170.

Champagne, M. J. 1957. Contribution a l'étude de la morphologie de la serumalbumine en solution étendue. *J. Chim. Phys.* 54:393–410.

Chuang, T. J., and K. B. Eisenthal. 1972. Theory of fluorescence depolarization by anisotropic rotational diffusion. *J. Chem. Phys.* 57: 5094–5097.

Curry, S., H. Mandelkow, P. Brick, and N. Franks. 1998. Crystal structure of human serum albumin complexed with fatty acid reveals an asymmetric distribution of binding sites. *Nat. Struct. Biol.* 5:827–828.

Duchowicz, R., M. L. Ferrer, and A. U. Acuña. 1998. Kinetic spectroscopy of erythrosin phosphorescence and delayed fluorescence in aqueous solution at room temperature. *Photochem. Photobiol.* 68:494–501.

Durchslang, H., and P. Zipper. 1997. Calculation of hydrodynamic parameters of biopolymers from scattering data using whole body approaches. *Prog. Colloid Polymer Sci.* 107:43–47.

Ehrenberg, M., and R. Rigler. 1972. Polarized fluorescence and rotational Brownian motion. *Chem. Phys. Lett.* 14:539–544.

Feng, L., J. D. Andrade, and C. Z. Hu. 1989. Scanning tunneling microscopy of proteins on graphite surfaces. *Scan. Microsc.* 3:399–410.

García de la Torre, J., and V. A. Bloomfield. 1981. Hydrodynamic properties of complex rigid biological macromolecules: theory and applications. *Q. Rev. Biophys.* 14:81–139.

García de la Torre, J., M. L. Huertas, and B. Carrasco. 2000. Calculation of hydrodynamic properties of globular proteins from their atomic-level structure. *Biophys. J.* 78:719–730.

García de la Torre, J., S. Navarro, C. López-Martínez, F. G. Díaz, and J. J. López-Cascales. 1994. HYDRO: a computer program for the prediction of hydrodynamic properties of macromolecules. *Biophys. J.* 67:530–531.

Garland, P. B., and C. H. Moore. 1979. Phosphorescence of protein-bound eosin and erythrosin. *Biochem. J.* 183:561–572.

Gentiu, M., M. Vincent, J. C. Brochon, A. K. Livesey, N. Cittanova, and J. Gallay. 1990. Time resolved fluorescence of the single tryptophan residue in rat α-fetoprotein and rat serum albumin: analysis by the maximum-entropy method. *Biochemistry.* 29:10405–10412.

Hagag, N., E. R. Birnbaum, and D. W. Darnall. 1983. Resonance energy transfer between cysteine-34, tryptophan-214, and tyrosine-411 of human serum albumin. *Biochemistry.* 22:2420–2427.

Harding, S. E. On the hydrodynamic analysis of macromolecular conformation. 1995. *Biophys. Chem.* 55:69–93.

He, X. M., and D. C. Carter. 1992. Atomic structure and chemistry of human serum albumin. *Nature.* 358:209–215.

Helms, M. K., C. E. Petersen, V. B. Nadhipuran, and D. M. Jameson. 1997. Time resolved studies on site-directed mutants of human serum albumin. *FEBS Lett.* 408:67–70.

Herman, J. R., T. R. Londo, N. A. Rahman, and B. G. Barisas. 1992. Normally-on photomultiplier gating circuit with reduced post-gate artifacts for use in transient luminescence measurements. *Rev. Sci. Instrum.* 63:5454–5458.

Ho, J. X., E. W. Holowachuk, E. J. Norton, P. D. Twigg, and D. C. Carter. 1993. X-ray and primary structure of horse serum albumin (*Equus caballus*) at 0.27 nm resolution. *Eur. J. Biochem.* 215:205–212.

Hustedt, E. J., C. E. Cobb, A. H. Beth, and J. M. Beechem. 1993. Measurement of rotational dynamics by the simultaneous nonlinear analysis of optical and EPR data. *Biophys. J.* 64:614–621.

Kinosita, K., Jr., S. Kawato, and A. Ikegami. 1977. A theory of fluorescence polarization decay in membranes. *Biophys. J.* 20:289–305.

Lakowicz, J. R. 1999. Principles of Fluorescence Spectroscopy, 2nd ed. Kluver Academic-Plenum Publishers, New York.

Lakowicz, J. R., and I. Gryzynski. 1992. Tryptophan fluorescence intensity and anisotropy decays of human serum albumin resulting from one-photon and two-photon excitation. *Biophys. Chem.* 45:1–6.

Lettinga, M. P., E. M. Klarenbeek, H. Zuilhof, and M. A. M. van Zandvoort. 1999. The orientation of the phosphorescence dipole moment of erythrosine B within its molecular frame. *J. Fluoresc.* 9:265–279.

Litovitz, T. A. 1952. Temperature dependence of the viscosity of associated liquids. *J. Chem. Phys.* 20:1088–1089.

Loeb, G. I., and H. A. Scheraga. 1956. Hydrodynamic and thermodynamic properties of bovine serum albumin at low pH. *J. Phys. Chem.* 60: 1633–1644.

Luft, A. J., and F. L. Lorscheider. 1983. Structural analysis of human and bovine alpha-fetoprotein by electron microscopy, image processing, and circular dichroism. *Biochemistry.* 22:5978–5981.

Marriott, G., T. M. Jovin, and Y. Yan-Marriott. 1994. Synthesis and spectroscopic characterization of 1-bromo-4-(bromoacetyl)naphtalene: a thiol-reactive phosphorescent probe. *Anal. Chem.* 66:1490–1494.

Marzola, P., and E. Gratton. 1991. Hydration and protein dynamics: frequency domain fluorescence on proteins in reverse micelles. *J. Phys. Chem.* 95:9488–9495.

Mateo, C. R., M. P. Lillo, J. C. Brochon, M. Martínez-Ripoll, J. Sanz-Aparicio, and A. U. Acuña. 1993. Rotational dynamics of 1,6-diphenyl-1,3,5-hexatriene and derivatives from fluorescence depolarization. *J. Phys. Chem.* 97:3486–3491.

Mateo, C. R., M. P. Lillo, J. González-Rodríguez, and A. U. Acuña. 1991. Molecular order and fluidity of the plasma membrane of human platelets from time-resolved fluorescence depolarization. *Eur. Biophys. J.* 20: 41–52.

Matulis, D., C. G. Baumann, V. A. Bloomfield, and R. E. Lovrien. 1999. 1-Anilino-8-naphthalene sulfonate as a protein conformational tightening agent. *Biopolymers.* 49:451–488.

McMillan, D. E. 1974. A comparison of five methods for obtaining the intrinsic viscosity of bovine serum albumin. *Biopolymers.* 13: 1367–1376.

Miner, C. S., and N. Dalton. 1953. Glycerol. Reinhold Publishing, New York.

Montejo, J. M., K. R. Naqvi, M. P. Lillo, J. González-Rodríguez, and A. U. Acuña. 1992. Conformation of human fibrinogen in solution from polarized triplet spectroscopy. *Biochemistry.* 31:7580–7586.

Munro, I., I. Pecht, and L. Stryer. 1979. Subnanosecond motions of tryptophan residues in proteins. *Proc. Natl. Acad. Sci. U.S.A.* 76:56–60.

Peng, H., and B. G. Barisas. 1997. Saturation effects on phosphorescence anisotropy measurements at high laser pulse energies. *J. Fluoresc.* 7:139–145.

Perrin, F. 1934. Mouvement brownien d'un ellipsoide: dispersion dielectrique pour des molecules ellipsoidales. *J. Phys. Radium Ser. VII.* 5:303–304.

Peters, T., Jr.1996. All About Albumin. Academic Press, New York.

Philo, J. S. 1994. Measuring sedimentation, diffusion and molecular weights of small molecules by direct fitting of sedimentation velocity concentration profiles. *In* Modern Analytical Ultracentrifugation. T. M. Shuster and T. M. Laue, editors. Birkhauser, Boston. 156–170.

Small, E. W., and I. Isenberg. 1977. Hydrodynamic properties of a rigid molecule: rotational and linear diffusion and fluorescence anisotropy. *Biopolymers.* 16:1907–1928.

Squire, P. G., P. Moser, and C. T. O'Konski. 1968. The hydrodynamic properties of bovine serum albumin monomer and dimer. *Biochemistry.* 7:4261–4271.

Sugio, S., A. Kashima, S. Mochizuki, N. Noda, and K. Kobayashi. 1999. Crystal structure of human serum albumin at 2.5 Å resolution. *Protein Eng.* 12:439–446.

Tanford, C., and J. G. Buzzel. 1956. The viscosity of aqueous solutions of bovine serum albumin between pH 4.3 and 10.5. *J. Phys. Chem.* 60: 225–231.

West, R. C. 1982–1983. Handbook of Chemistry and Physics. CRC Press, Boca Raton, FL.

Wahl, P. 1983. Fluorescence anisotropy decay and Brownian rotational motion: theory and application in biological systems. *In* Time-Resolved Fluorescence Spectroscopy in Biochemistry and Biology. R. B. Cundall and R. E. Dale, editors. NATO ASI Series A69. Plenum Press, New York. 497–521.

Yoshida, T. M., T. M. Jovin, and B. G. Barisas. 1989. A high-speed photomultiplier gating circuit for luminescence measurements. *Rev. Sci. Instrum.* 60:2924–2928.